Hindawi
International Journal of Mathematics and Mathematical Sciences
Volume 2024, Article ID 6069996, 17 pages
https://doi.org/10.1155/2024/6069996

Review Article

Analysis of COVID-19 Disease Model: Backward Bifurcation and Impact of Pharmaceutical and Nonpharmaceutical Interventions

Ibad Ullah,[1] Nigar Ali,[1] Ihtisham Ul Haq,[1] Imtiaz Ahmad,[1] Mohammed Daher Albalwi,[2] and Md. Haider Ali Biswas[3]

[1]*Department of Mathematics, University of Malakand, Chakdara 18000, Khyber Pakhtunkhwa, Pakistan*
[2]*Yanbu Industrial College, The Royal Commission for Jubail and Yanbu, Yanbu 30436, Saudi Arabia*
[3]*Khulna University, Khulna 9208, Bangladesh*

Correspondence should be addressed to Md. Haider Ali Biswas; mhabiswas@yahoo.com

Received 4 February 2024; Revised 18 March 2024; Accepted 25 March 2024; Published 5 April 2024

Academic Editor: Kareem T. Elgindy

Copyright © 2024 Ibad Ullah et al. This is an open access article distributed under the Creative Commons Attribution License, which permits unrestricted use, distribution, and reproduction in any medium, provided the original work is properly cited.

The SEIQHR model, introduced in this study, serves as a valuable tool for anticipating the emergence of various infectious diseases, such as COVID-19 and illnesses transmitted by insects. An analysis of the model's qualitative features was conducted, encompassing the computation of the fundamental reproduction number, R_0. It was observed that the disease-free equilibrium point remains singular and locally asymptotically stable when $R_0 < 1$, while the endemic equilibrium point exhibits uniqueness when $R_0 > 1$. Additionally, specific conditions were outlined to guarantee the local asymptotic stability of both equilibrium points. Employing numerical simulations, the graphical representation illustrated the influence of model parameters on disease dynamics and the potential for its eradication across different noninteger orders of the Caputo derivative. In essence, the adoption of a fractional epidemic model contributes to a deeper comprehension and enhanced biological insights into the dynamics of diseases.

1. Introduction

In December 2019, an enigmatic pneumonia outbreak traced back to a market in Wuhan caught global attention, prompting swift action from the World Health Organization (WHO) [1–4]. By January 7, 2020, scientists identified a novel strain within the coronavirus family as the culprit behind the outbreak, dubbing it COVID-19 [5]. This discovery marked the beginning of a tumultuous journey as the virus swiftly spread, culminating in WHO declaring it a pandemic on March 12, 2020. The symptoms of COVID-19, ranging from fever to breathing difficulties, captured the world's concern. What intrigued scientists even more was the fact that some carriers showed no symptoms yet could unknowingly spread the virus [6–8].

As the world grappled with the unfolding crisis, mathematical models emerged as indispensable tools in understanding and managing infectious diseases [9–11]. Researchers worldwide rushed to develop and refine compartmental models to dissect the dynamics of the COVID-19 epidemic [12, 13]. Notably, Yang and Wang [14] presented a comprehensive model that accounted for various transmission pathways of the coronavirus. Their findings underscored the critical role of environmental factors in shaping disease transmission dynamics, emphasizing the need for sustained intervention efforts and preventive measures.

In China, Li et al. [15] crafted an SEIQR model tailored to the COVID-19 epidemic, offering insights into the impact of timely lockdowns on controlling case counts. Meanwhile, Ngonghala et al. [16] focused their attention on America, particularly New York, to evaluate the effectiveness of mitigation strategies such as social distancing and mask-wearing. Eikenberry et al. [17] explored the community-wide effects of mask-wearing among asymptomatic individuals, shedding light on its potential in curbing transmission rates.

While existing studies primarily relied on integer-order differential equations to model epidemic dynamics, recent advances have highlighted the promise of fractional-order models [18, 19]. These models offer a broader perspective by

incorporating nonlocal behaviors, potentially revolutionizing our understanding of complex phenomena [20–22].

The structure of our paper is as follows: section 1 lays the groundwork, while section 2 outlines the model formulation. Sections 3 and 4 delve into foundational and stability analyses, respectively. Sections 5 and 6 explore sensitivity analysis, followed by bifurcation analysis and optimal control strategies in sections 7 and 8. In section 8, we elucidate the concept of fractional derivatives. Finally, sections 9 and 10 present numerical simulations, validating our analytical findings and concluding with a discussion and final remarks.

2. Model Framework

In the SEIQHR model, the population is categorized into six groups: susceptible (S), exposed (E), infected (I), quarantine (Q), hospitalised (H), and recovered (R).

$$\begin{cases} \dot{S} = \Lambda - \beta IS - \mu S, \\ \dot{E} = \beta IS - (\pi + \mu)E, \\ \dot{I} = \pi E - (\mu + \gamma + \psi + \eta)I, \\ \dot{Q} = (1-\delta)\gamma I - (\phi + \tau + \mu)Q, \\ \dot{H} = \tau Q + \psi I - (\mu + \kappa + \sigma)H, \\ \dot{R} = \delta\gamma I + \phi Q + \kappa H - \mu R. \end{cases} \tag{1}$$

Starting from the subsequent initial conditions: $S(0) = S_0 > 0, E(0) = E_0, I(0) = I_0, Q(0) = Q_0, H(0) = H_0, R(0) = R_0 \geq 0$.

Table 1 shows the descriptions of the parameter, while the dynamics of COVID-19 transmission are illustrated in the flowchart depicted in Figure 1.

COVID-19 spreads among susceptible individuals at a rate denoted by β due to contact with infected individuals. Exposed individuals transition to the infected group at a rate represented by π. Upon infection, individuals either enter quarantine or recover. A portion $(1-\delta)$ of infected individuals moves to the quarantine category at a rate of γ, while the remaining $\delta\gamma$ transition to the recovered category upon recovery.

3. Analysis of the Model

In this section, we look at some of the most noteworthy results from the model (1) analysis. By summing all of their equations, we may get the complete dynamics of the system (1) given by

$$\frac{dN}{dt} = \Lambda - \mu N - \eta I - \sigma H \leq \Lambda - \mu N. \tag{2}$$

We obtain the following conclusion after solving the preceding (2):

$$N(t) = N_0 e^{-\mu t} + \frac{\Lambda}{\mu}\left(1 - e^{-\mu t}\right). \tag{3}$$

The (3) converges to Λ/μ as t approaches infinity. Moreover, it asserts the nonnegativity of variables within the model (1) for all $t \geq 0$. Consequently, the initial solution (1) of the model will maintain positivity for any $t \geq 0$.

3.1. Positivity and Boundedness. Next, we attempt to demonstrate the model's solution positivity and boundedness of the model (1).

Theorem 1. *The compartments of the model (1) at $t = 0$ $(S_0 > 0, E_0 > 0, I_0 > 0, Q_0 > 0, H_0 > 0, R_0 > 0)$, and then, the solution for $t > 0$ of all the variables in the model will be nonnegative.*

Proof. To demonstrate the outcome, begin with the models (1),

$$\begin{aligned} \frac{dS}{dt} &= \Lambda - \varphi(t) - \mu S \\ &\geq -(\varphi(t) + \mu)S, \end{aligned} \tag{4}$$

where $\varphi(t) = \beta I$. We get the following result after integrating:

$$S(t) \geq S_0 e^{-\int_0^t (\varphi(\tau) + \mu) d\tau} > 0. \tag{5}$$

We can simply continue the preceding technique to demonstrate the positivity of the model (1) remaining variables.

To demonstrate the boundedness of the system's solution (1), we noted in the preceding theorem that the solution is nonnegative, and we can use (3) to show that the solution is bounded when $t \longrightarrow \infty$ is Λ/μ. □

3.2. Disease-Free Equilibrium Points and Basic Reproduction Number. We can readily express our E_0 by just setting the disease classes and derivatives to zero in model (1); it would take the form $E_0 = (\Lambda/\mu, 0, 0, 0, 0, 0)$.

To calculate the model's basic reproduction number, we propose utilising a next-generation matrix. For that, we take the disease classes from our model as follows:

$$\begin{aligned} \dot{E}(t) &= \beta IS - (\alpha + \mu)E, \\ \dot{I}(t) &= \alpha E - (\mu + \gamma + \psi + \eta)I, \\ \dot{Q}(t) &= \gamma(1-\delta)I - (\phi + \tau + \mu)Q, \\ \dot{H}(t) &= \tau Q + \psi I - (\kappa + \sigma + \mu)H. \end{aligned} \tag{6}$$

From system (6), we develop matrix F and V as follows:

$$F = \begin{pmatrix} \beta \mathrm{SI} \\ 0 \\ 0 \\ 0 \end{pmatrix} \text{and,}$$

$$V = \begin{pmatrix} -(\mu + \pi) \\ \pi E - (\gamma + \mu + \eta + \psi)I \\ \gamma(1-\delta)I - (\phi + \tau + \mu)Q \\ \tau Q + \psi I - (\kappa + \sigma + \mu) \end{pmatrix}. \tag{7}$$

Table 1: Parameters and their descriptions of the system (1).

Variable	Interpretation
Λ	The recruitment rate of susceptible individuals
β	The effectual contact rate among susceptible and infectious individuals
μ	Death rate of individuals (natural)
π	The rate of exposed individuals becoming infectious
τ	The rate of quarantined individuals becoming hospitalised
$(1-\delta)$	The portion of infected individuals
γ	The recovery rate of infected ones

The Jacobian matrices corresponding to F and V at the disease-free equilibrium (DFE) are denoted by F^* and V^*, respectively.

$$F^* = \begin{pmatrix} 0 & \frac{\Lambda\beta}{\mu} & 0 & 0 \\ 0 & 0 & 0 & 0 \\ 0 & 0 & 0 & 0 \\ 0 & 0 & 0 & 0 \end{pmatrix} \text{ and}$$

$$V^* = \begin{pmatrix} \mu+\pi & 0 & 0 & 0 \\ \pi & \gamma+\mu+\eta+\psi & 0 & 0 \\ 0 & -\gamma(1-\delta) & \phi+\tau+\mu & 0 \\ 0 & -\psi & -\tau & \sigma+\kappa+\mu \end{pmatrix}. \tag{8}$$

Hence, F^*V^{*-1} represents the next-generation matrix of the system (1). Therefore, $R_0 = \rho(F^*V^{*-1})$, where ρ denotes the spectral radius of the next-generation matrix F^*V^{*-1}.

So, $\rho(F^*V^{*-1}) = \pi\beta\Lambda/\mu(\mu+\pi)(\mu+\gamma+\eta+\psi) = R_0$. Therefore,

$$R_0 = \frac{\pi\beta\Lambda}{\mu(\mu+\pi)(\mu+\gamma+\eta+\psi)}. \tag{9}$$

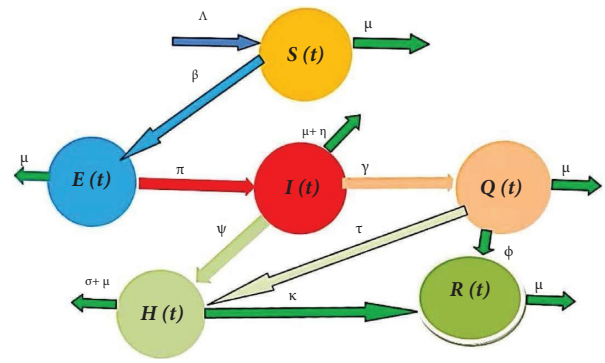

Figure 1: Flow diagram of the COVID-19 model (1).

Figure 2 represents the dynamics of R_0 with respect to the transmission rates π and γ.

4. Local and Global Stability Analyses

Theorem 2. *When $R_0 < 1$, the disease-free equilibrium exhibits local asymptotic stability.*

Proof. The Jacobian matrix associated with the system (1) at the disease-free equilibrium (E_o) is outlined as follows:

$$\mathrm{JE}_0 = \begin{pmatrix} -\mu & 0 & -\frac{\beta\Lambda}{\mu} & 0 & 0 & 0 \\ 0 & -(\pi+\mu) & \frac{\beta\Lambda}{\mu} & 0 & 0 & 0 \\ 0 & \pi & -(\mu+\gamma+\eta+\psi) & 0 & 0 & 0 \\ 0 & 0 & (1-\delta)\gamma & -(\mu+\tau+\phi) & 0 & 0 \\ 0 & 0 & \psi & \tau & -(\mu+\kappa+\sigma) & 0 \\ 0 & 0 & \delta\gamma & \phi & \kappa & -\mu \end{pmatrix}. \tag{10}$$

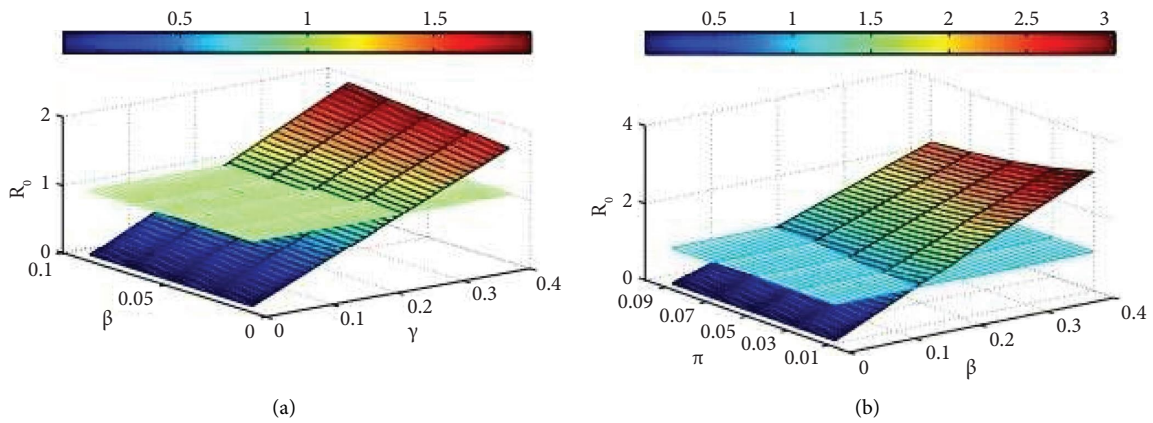

FIGURE 2: The dynamics of R_0 with respect to the transmission rates β, π, and γ. (a) The change in the value of R_0 concerning the transmission rates β and γ. (b) Impact of β and π on R_0.

The eigenvalue of the above Jacobian matrix at E_o is

$$\begin{aligned}
\lambda_1 &= -\mu,\\
\lambda_2 &= -(\mu+\pi),\\
\lambda_3 &= -(\mu+\gamma+\eta+\psi),\\
\lambda_4 &= -(\tau+\phi+\mu),\\
\lambda_5 &= -(\kappa+\sigma+\mu),\\
\lambda_6 &= -\mu.
\end{aligned} \tag{11}$$

So, all the eigenvalues are negative which complete the proof. □

Theorem 3. *If $R_0 < 1$, the disease-free equilibrium demonstrates global stability.*

Proof. We partition system (1) into two compartments: uninfected and infected individuals, represented as follows:

$$\begin{aligned}
\frac{dX}{dt} &= F(X,\mathcal{F}),\\
\frac{d\mathcal{F}}{dt} &= M(X,\mathcal{F}), M(X,0) = 0.
\end{aligned} \tag{12}$$

The point $E_0 = (N_0, 0)$ is globally asymptotically stable equilibrium of system (1) if the following conditions are satisfied:

L_1: E_0 is globally asymptotically stable for

$$\frac{dX}{dt} = F(X,0)\, L_2\colon \overline{M}(X,\mathcal{F}) \geq 0,\ (X,Z)\varepsilon\Omega, \tag{13}$$

where $M(X,\mathcal{F}) = A\mathcal{F} - \overline{M}(X,\mathcal{F}), A = D_{\mathcal{F}}M(N_0,0)$ is a Metzler matrix.

Thus, we have

$$\begin{aligned}
\frac{dX}{dt} &= \begin{pmatrix} \Lambda - \beta SI - \mu S \\ \phi Q + \delta\gamma I + \kappa H - \mu R \end{pmatrix}.\\
F(X,0) &= \begin{pmatrix} \Lambda - \beta SI - \mu S \\ \phi Q + \delta\gamma I + \kappa H - \mu R \end{pmatrix}.\\
\frac{d\mathcal{F}}{dt} = M(X,\mathcal{F}) &= \begin{pmatrix} \beta SI - (\mu+\alpha)E \\ \pi E - (\mu+\gamma+\eta+\psi) \\ \gamma(1-\delta)I - (\phi+\tau+\mu)Q \\ \text{tauQ} + \text{psiI} - (\kappa+\sigma+\mu) \end{pmatrix}.
\end{aligned} \tag{14}$$

Therefore, given $M(X,0) = 0$, the equilibrium $N_0 = (\Lambda/\mu, 0)$ is globally asymptotically stable for $dX/dt = F(X,0)$.

$$\begin{aligned}
L_1\colon \frac{dX}{dt} &= F(X,0)\\
&= \begin{pmatrix} \beta SI - (\mu+\pi)E \\ \pi E - (\mu+\gamma+\eta+\psi) \\ (1-\delta)\gamma I - (\phi+\tau+\mu)Q \\ \tau Q + \psi I - (\kappa+\sigma+\mu) \end{pmatrix}.
\end{aligned} \tag{15}$$

When solved for L_2, it results in

$$A = F^* - V^* = \begin{pmatrix} -(\mu+\pi) & \frac{\Lambda\beta}{\mu} & 0 & 0 \\ \pi & -(\mu+\eta+\gamma+\psi) & 0 & 0 \\ 0 & (1-\delta)\gamma & -(\tau+\phi+\mu) & 0 \\ 0 & \psi & \tau & -(\kappa+\mu+\sigma) \end{pmatrix}, \tag{16}$$

with $A\mathcal{F}$ is given by

$$A\mathcal{F} = \left(-(\mu+\pi)E + \frac{\beta\Lambda I}{\mu}\pi E - (\mu+\gamma+\eta+\psi)I\gamma(1-\delta)I - (\tau+\phi+\mu)Q\psi I + \tau Q - (\kappa+\sigma+\mu) \right). \tag{17}$$

Thus,

$$(\overline{M}(X,\mathcal{F})) = \begin{pmatrix} 0 \\ 0 \\ 0 \\ 0 \end{pmatrix} = \begin{pmatrix} \overline{M_1}(X,\mathcal{F}) \\ \overline{M_2}(X,\mathcal{F}) \\ \overline{M_2}(X,\mathcal{F}) \\ \overline{M_4}(X,\mathcal{F}) \end{pmatrix}, \tag{18}$$

Since $\overline{M_1}(X,\mathcal{F}) = 0$, $\overline{M_2}(X,\mathcal{F}) = 0, \overline{M_3}(X,\mathcal{F}) = 0$, and $\overline{M_4}(X,\mathcal{F}) = 0$, we have $\overline{G}(X,\mathcal{F}) \geq 0$ for $(X,\mathcal{F})\varepsilon\Omega$.

Therefore, E_0 is globally asymptotically stable if $R_0 < 1$. □

4.1. Existence of Endemic Equilibrium Point. In this section, we investigate the potential existence of an endemic equilibrium denoted as $\mathcal{E}^* = (S^*, E^*, Q^*, I^*, H^*, R^*)$.

This endemic equilibrium is

$$\begin{aligned} S^* &= \frac{\Lambda}{\beta I^* + \mu}, \\ E^* &= \frac{\beta\Lambda I^*}{(\mu+\pi)(\beta I^* + \mu)}, \\ I^* &= \frac{\mu}{\beta}(R_0 - 1), \\ Q^* &= \frac{\gamma\mu(1-\delta)}{\beta(\tau+\phi+\mu)}(R_0 - 1), \\ H^* &= \frac{(\tau+\phi+\mu)\psi I^* + \tau\gamma(1-\delta)I^*}{(\kappa+\sigma+\mu)(\tau+\phi+\mu)}, \\ R^* &= \frac{g_1\{\phi g_3 I^* + g_2\gamma\delta I^*\} + \kappa\{g_2\psi I^* + \tau g_3 I^*\}}{g_1 g_2 \mu}, \end{aligned} \tag{19}$$

where $g_1 = \kappa + \sigma + \mu$, $g_2 = \tau + \phi + \mu$, and $g_3 = \gamma(1-\delta)$.

4.2. Local and Global Stability of $\mathcal{E}^*$

Theorem 4. *The local asymptotic stability of the endemic equilibrium $\mathcal{E}^*$ occurs when $R_0 > 1$.*

Proof. The Jacobian matrix corresponding to the system (1) is outlined as follows:

$$J = \begin{pmatrix} -\beta I^* - \mu & 0 & -\beta S^* & 0 & 0 & 0 \\ \beta I^* & -(\mu+\pi) & \beta S^* & 0 & 0 & 0 \\ 0 & \pi & -(\mu+\gamma+\eta+\psi) & 0 & 0 & 0 \\ 0 & 0 & \gamma(1-\delta) & -(\phi+\tau+\mu) & 0 & 0 \\ 0 & 0 & \psi & \tau & -(\kappa+\sigma+\mu) & 0 \\ 0 & 0 & \delta\gamma & \phi & \kappa & -\mu \end{pmatrix}. \tag{20}$$

The eigenvalues of the above matrix at $\mathscr{E}^*$ are given as follows:

$$\begin{aligned} \lambda_1 &= -\mu, \\ \lambda_2 &= -(\psi+\gamma+\mu+\eta), \\ \lambda_3 &= -(\phi+\tau+\mu), \\ \lambda_4 &= -(\sigma+\kappa+\mu). \end{aligned} \tag{21}$$

The quadratic expression $\lambda^2 + \mu(\mu+\pi)R_0(\lambda+1)$ consists solely of nonnegative terms, ensuring that all its roots are negative, i.e., $\lambda_{5,6} < 0$. This concludes the proof. □

Theorem 5. *The endemic equilibrium state* $\mathscr{E}^* = (S^*, E^*, I^*, Q^*, H^*, R^*)$ *within model (1) achieves global asymptotic stability if* $R_0 < 1$*; otherwise, it becomes unstable.*

We obtained a Lyapunov function to demonstrate the global stability of the model at the endemic equilibrium point $\mathscr{E}^* = (S^*, E^*, I^*, Q^*, H^*, R^*)$.

$$\frac{d\Psi}{dt} = \left[(S-S^*) + (E-E^*) + (I-I^*) + (Q-Q^*) + (H-H^*)\right] \times \mu R_0 S^* - \mu S - \mu E - g_1 I - g_2 Q - g_3 H. \tag{22}$$

Here, $g_1 = \mu + \eta + \delta\gamma$, $g_2 = \mu + \phi$ and $g_3 = \mu + \delta + \kappa$.

$$\frac{d\Psi}{dt} = -\left[(S-S^*) + (E-E^*) + (I-I^*) + (Q-Q^*) + (H-H^*)\right] \times \left[\mu(S - R_0 S^*) + \mu E + g_1 I + g_2 Q + g_3 H\right]. \tag{23}$$

Hence, $d\Psi/dt \le 0$ for all $(S^*, E^*, I^*, Q^*, H^*, R^*)$. The equality $d\Psi/dt = 0$ holds only for $S^*, E^*, I^*, Q^*, H^*, R^*$.

As a result, positive $\mathscr{E}^*$ is globally asymptotically stable.

5. Sensitivity Analysis

In this section, sensitivity analysis is utilized to evaluate the importance of the generic parameters contributing to the basic reproduction number R_0. Parameters demonstrating a positive impact are deemed highly and proportionally sensitive to the value of R_0, while those with a negative impact are less responsive to a decrease in R_0. Additionally, there is a category of parameters termed neutrally sensitive. The sensitivity index method is utilized to identify the most critical model parameters, where those with a positive sign are deemed highly sensitive to the value of R_0, maintaining a proportional relationship with it.

$$\Upsilon_{hi}^{R_0} = \frac{\partial R_0}{\partial h_i} \times \frac{h_i}{R_0}, \tag{24}$$

where R_0 is the fundamental reproduction ratio and *Pi* is as mentioned before. Using the stated formula, we arrive at

$$\begin{aligned}
\Upsilon_{\Lambda} &= 1,\\
\Upsilon_{\beta} &= 1,\\
\Upsilon_{\eta} &= -\frac{\eta}{\gamma+\mu+\eta+\psi},\\
\Upsilon_{\gamma} &= -\frac{\gamma}{\gamma+\mu+\eta+\psi},\\
\Upsilon_{\pi} &= \frac{\mu}{\mu+\pi},\\
\Upsilon_{\psi} &= -\frac{\psi}{\gamma+\mu+\eta+\psi},\\
\Upsilon_{\mu} &= -\frac{(2\mu+\pi)(\mu+\gamma+\eta+\psi)-\mu(\mu+\alpha)}{\mu(\mu+\pi)(\mu+\gamma+\eta+\psi)}.
\end{aligned} \tag{25}$$

Some criteria have been shown to be positive, while others have been found to be negative. A positive relationship between the parameters indicates that raising the value of that parameter has a substantial influence on the frequency of disease transmission. A negative link indicates that increasing the relevance of these criteria might assist in reducing the disease's aggressiveness. The physical appearance of the number signals is given in Figure 3.

6. Bifurcation Analysis

To investigate whether the model system (1) exhibits backward bifurcation, we apply the theory of center manifolds following the methodology described by Castillo–Chavez and Song in [6]. We consider the system as follows: $dx/dt = f(x,\beta^*)$, where f is continuously differentiable at least twice in x and β denotes the bifurcation parameters. The equations a and b are represented as follows:

$$\begin{aligned}
a &= \sum_{k,i,j=1}^{6} v_k w_i w_j \frac{\partial^2 g_k}{\partial u_i \partial u_j}(E_0,\beta^*) \text{ and,}\\
b &= \sum_{k,i,j=1}^{6} v_k w_i \frac{\partial^2 g_k}{\partial u_i \partial_{\beta}}(E_0,\beta^*).
\end{aligned} \tag{26}$$

Therefore, when $a>0$ and $b>0$, backward bifurcation occurs, whereas when $a<0$ and $b>0$, forward bifurcation occurs.

Now, to calculate the bifurcation parameter β, then R_0 be equivalent to

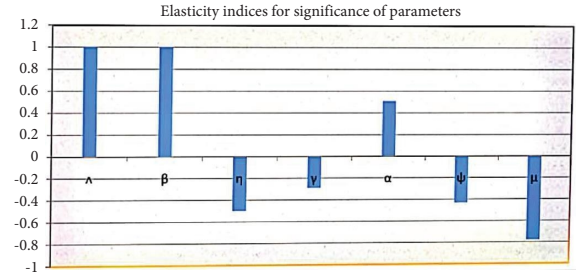

Figure 3: Elasticity indices for significance of parameters in R_0.

$$\begin{aligned}
\beta &= \beta^*\\
&= \frac{\mu(\mu+\pi)(\mu+\gamma+\eta+\psi)}{\pi\Lambda},
\end{aligned} \tag{27}$$

by setting $S = x_1, E = x_2, I = x_3, Q = x_4, H = x_5$, and $R = x_6$, the model system (1) can be rewritten in the following form:

$$\begin{aligned}
g_1(x) &= \Lambda - x_1 x_3 \beta - x_1 \mu,\\
g_2(x) &= x_1 x_3 \beta - (\pi+\mu)x_2,\\
g_3(x) &= \pi x_2 - (\gamma+\mu+\psi+\eta)x_3,\\
g_4(x) &= (1-\delta)\gamma x_3 - (\phi+\tau+\mu)x_4,\\
g_5(x) &= \psi x_3 + \tau x_4 - (\kappa+\sigma+\mu)x_5,\\
g_6(x) &= \phi x_4 + \kappa x_5 + \delta\gamma x_3 - \mu x_6.
\end{aligned} \tag{28}$$

The Jacobian matrix of the model system (28) was assessed at E_0 with $\beta = \beta^*$. This assessment yielded both the right and left eigenvectors associated with a single zero eigenvalue.

$$\begin{aligned}
u_1 &= \frac{\beta^* \Lambda}{\mu^2} u_3,\\
u_2 &= \frac{\mu+\gamma+\eta+\psi}{\alpha} u_3,\\
u_4 &= \frac{\gamma(1-\delta)}{\tau+\mu+\phi} u_3,\\
u_5 &= \frac{\psi k_1 + \tau\gamma k_3}{k_1 k_2} u_3,\\
u_6 &= \frac{k_1 k_2 \delta\gamma + k_2 k_3 \phi\gamma + \kappa k_1 \psi + k_3 \tau\gamma}{\mu k_1 k_2} u_3,
\end{aligned} \tag{29}$$

where $k_1 = \mu+\tau+\phi, k_2 = \kappa+\sigma+\mu$, and $k_3 = 1-\delta$. With $v_1 = 0$, $v_3 = \mu + \pi/\pi v_2$, $v_4 = 0$, $v_5 = 0$, and $v_6 = 0$.

The nonzero partial derivatives are derived as follows:

$$\frac{\partial^2 g_2}{\partial x_1 \partial x_3} = \beta^*,$$

$$\frac{\partial^2 g_2}{\partial x_3 \partial x_1} = \beta^*,$$

$$\frac{\partial^2 g_2}{\partial x_1 \partial \beta^*} = 0,$$

$$\frac{\partial^2 g_2}{\partial x_3 \partial \beta^*} = \frac{\Lambda}{\mu}, \tag{30}$$

$$\delta = \frac{\Lambda v_2 u_3}{\mu},$$

$$a = \frac{2v_2 \beta^* \Lambda u_3^2}{\mu^2},$$

$$b = \frac{\Lambda v_2 u_3}{\mu}.$$

As $a > 0$ and $b > 0$, hence the model exhibits the backward bifurcation.

The observation depicted in Figure 4 indicates that model (1) exhibits the phenomenon of backward bifurcation when $R_0 = 1$.

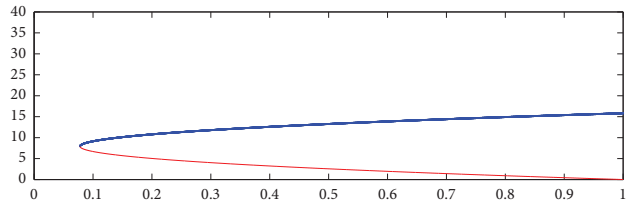

Figure 4: Bifurcation diagram of model (1) showing backward bifurcation.

7. Optimal Control Problem

The sensitivity analysis presented in the preceding part aids us in developing an effective control plan to combat this pandemic. We rebuild the model (1) by monitoring the most relevant factors in order to examine the effect of control measures on the future scenario. The model (1) has the following structure with the addition of two controls:

$$\begin{cases} \dot{S}(t) = \Lambda - (1-u_1)\beta SI - \mu S, \\ \dot{E}(t) = (1-u_1)\beta SI - (\pi + \mu + \rho u_2)E, \\ \dot{I}(t) = \pi E - (\mu + \gamma + \psi + \eta)I, \\ \dot{Q}(t) = \gamma(1-\delta)I - (\tau + \phi + \mu)Q + \rho u_2 E, \\ \dot{H}(t) = \psi I + \tau Q - (\kappa + \sigma + \mu)H, \\ \dot{R}(t) = \phi Q + \delta\gamma I + \kappa H - \mu R, \end{cases} \tag{31}$$

with the given initial conditions

$$S(0) > 0 \text{ and } E(0), I(0), Q(0), H(0)R(0) \geq 0. \tag{32}$$

The control $u_1(t)$ denotes cautious actions such as social isolation and frequent usage of face masks. Control $u_2(t)$ indicates a rapid step to isolate persons infected with the COVID-19 virus. We develop the functional objectives. J. Its goal is to reduce infectious persons while also lowering the cost of implemented controls u_1 and u_2.

$$J(u_1(t), u_2(t)) = \int_0^t \left\{ C_1 E(t) + C_2 I(t) + C_3 Q(t) + \frac{1}{2}\left(C_4 u_1^2(t) + C_5 u_2^2(t)\right) \right\} dt, \tag{33}$$

where C_1, C_2, C_3, C_4, and C_5 represent the weight constants.

Furthermore, in order to minimise the objective functional, we must determine the best control pair $u_1^*(t)$ and $u_2^*(t)$.

$$J\{u_1^*(t), u_2^*(t)\} = \min\{J(u_1(t), u_2(t)), u_1(t), u_2(t)\varepsilon U\}. \tag{34}$$

Given the system (31) and the control set $U = \{(u_1(t), u_2(t))\backslash u_i(t)\}$ is Lebesgue measurable on $[0,1], 0 \leq u_i(t) \leq 1$, $i = \{1, 2, 3\}$.

7.1. Existence of the Optimal Control Problem. This subsection gives proof that the control problem exists. The optimal control problem is given by the following equation in the Lagrangian:

$$L\{E, I, Q, u_1, u_2\} = C_1 E + C_2 I + C_3 Q + \frac{1}{2}C_4 u_1^2 + \frac{1}{2}C_5 u_2^2. \tag{35}$$

To get the smallest Lagrangian value, we define Hamiltonian H for the optimum control problem as follows:

$$H = L(E, I, Q, u_1, u_2) + \xi_1 \frac{dS(t)}{dt} + \xi_2 \frac{dE}{dt} + \xi_3 \frac{dI}{dt} + \xi_4 \frac{dQ}{dt} + \xi_5 \frac{dH}{dt} + \xi_6 \frac{dR}{dt}. \tag{36}$$

Adjoint variables $\xi_1, \xi_2, \xi_3, \xi_4, \xi_5$, and ξ_6 and optimal control variables u_1 and u_2.

$$\begin{aligned}
\xi_1'(t) &= -\{(\xi_2 - \xi_1)(1 - u_1)\beta I + \xi_1 \mu\},\\
\xi_2'(t) &= -\{C_1 - \xi_1(\mu + \alpha + \rho u_2) + \xi_3 \pi + \xi_4 \rho u_2\},\\
\xi_3'(t) &= -\{C_2 + (\xi_2 - \xi_1)(1 - u_1)\beta S - \xi_3(\mu + \gamma + \eta + \psi) + \xi_4 \gamma(1 - \delta) + \xi_5 \psi + \xi_6 \delta \gamma\},\\
\xi_4'(t) &= -\{C_3 - \xi_4(\tau + \phi + \mu) + \xi_5 \tau + \xi_6 \phi\},\\
\xi_5'(t) &= -\{-\xi_5(\kappa + \sigma + \mu) + \xi_6 \kappa\},\\
\xi_6'(t) &= -\{-\xi_6 \mu\},\\
u_1(t) &= \left\{\frac{(\xi_2 - \xi_1)\beta S I}{C_4}\right\},\\
u_2(t) &= \left\{\frac{(\xi_2 - \xi_4)\rho E}{C_5}\right\}.
\end{aligned} \tag{37}$$

Theorem 6. *For control problem (31), there exists* $u^*(t) = (u_1^*(t), u_2^*(t)) \varepsilon U$ *such that*

$$\min_{(u_1(t), u_2(t)) \varepsilon U} J(u_1(t), u_2(t)) = J(u_1^*, u_2^*). \tag{38}$$

By definition, the set of control variables $u_1, u_2 \varepsilon U$ is convex and closed. This optimum system has been defined, and it gives assurance regarding the solidity required for the optimal control system's validation. As a result, we discovered an optimum solution to our presented control issue. In order to solve our stated issue, we use the Pontryagin maximal approach. By using this principle, the Hamiltonian is given by

$$H = L(E, I, Q, u_1, u_2) + \xi_1 \frac{dS}{dt} + \xi_2 \frac{dE}{dt} + \xi_3 \frac{dI}{dt} + \xi_4 \frac{dQ}{dt} + \xi_5 \frac{dH}{dt} + \xi_6 \frac{dR}{dt}. \tag{39}$$

An existent nontrivial vector function $\xi = (\xi_1, \xi_2, \ldots, \xi_n)$ emerges if we designate (y^*, u^*) as an optimal solution to our formulated optimal control problem.

$$\begin{aligned}
\frac{dy}{dt} &= \frac{\partial H(t, y, u, \xi)}{\partial u},\\
0 &= \frac{\partial H(t, y, u, \xi)}{\partial u},\\
\xi'(t) &= \frac{\partial H(t, y, u, \xi)}{\partial u}.
\end{aligned} \tag{40}$$

These findings are achieved by applying the necessary conditions to the Hamiltonian.

Theorem 7. *With the provided optimal controls* u_1^* *and* u_2^*, *as well as the solutions* $S^*, E^*, I^*, Q^*, H^*, R^*$ *from the corresponding state system (31), the existence of adjoint variables* ξ_m *for* $m = 1, \ldots, 6$ *is assured.*

$$\begin{aligned}
\xi_1'(t) &= -\{(\xi_2 - \xi_1)(1 - u_1)\beta I + \xi_1 \mu\},\\
\xi_2'(t) &= -\{C_1 - \xi_1(\mu + \alpha + \rho u_2) + \xi_3 \pi + \xi_4 \rho u_2\},\\
\xi_3'(t) &= -\{C_2 + (\xi_2 - \xi_1)(1 - u_1)\beta S - \xi_3(\mu + \gamma + \eta + \psi) + \xi_4 \gamma(1 - \delta) + \xi_5 \psi + \xi_6 \delta \gamma\},\\
\xi_4'(t) &= -\{C_3 - \xi_4(\tau + \phi + \mu) + \xi_5 \tau + \xi_6 \phi\},\\
\xi_5'(t) &= -\{-\xi_5(\kappa + \sigma + \mu) + \xi_6 \kappa\},\\
\xi_6'(t) &= -\{-\xi_6 \mu\},
\end{aligned} \tag{41}$$

with transversality conditions $\xi_m(t) = 0, m = 1, 2, \ldots, 6$.

Proof. When considering the values S^*, E^*, I^*, Q^*, H^*, and R^* and computing the Hamiltonian's derivatives concerning the state variables $S(t), E(t), I(t), Q(t), H(t)$, and $R(t)$, we derive the subsequent adjoint system:

$$\begin{aligned}
\xi_1'(t) &= -\{(\xi_2 - \xi_1)(1 - u_1)\beta I + \xi_1\mu\},\\
\xi_2'(t) &= -\{C_1 - \xi_1(\mu + \alpha + \rho u_2) + \xi_3\pi + \xi_4\rho u_2\},\\
\xi_3'(t) &= -\{C_2 + (\xi_2 - \xi_1)(1 - u_1)\beta S - \xi_3(\mu + \gamma + \eta + \psi) + \xi_4\gamma(1 - \delta) + \xi_5\psi + \xi_6\delta\gamma\},\\
\xi_4'(t) &= -\{C_3 - \xi_4(\tau + \phi + \mu) + \xi_5\tau + \xi_6\phi\},\\
\xi_5'(t) &= -\{-\xi_5(\kappa + \sigma + \mu) + \xi_6\kappa\},\\
\xi_6'(t) &= -\{-\xi_6\mu\}.
\end{aligned} \tag{42}$$

with transversality conditions $\xi_m(t) = 0, m = 1, 2, \ldots, 6$. □

Theorem 8. *The pair of controls* (u_1^*, u_2^*)*, which optimizes the objective functional* J *within the region* U*, is expressed as follows:*

$$\begin{aligned}
u_1^* &= \max\left\{\min\left\{\frac{(\xi_2 - \xi_1)\beta\mathrm{SI}}{C_4}, 1\right\}, 0\right\},\\
u_2^* &= \max\left\{\min\left\{\frac{(\xi_2 - \xi_4)\rho E}{C_5}, 1\right\}, 0\right\}.
\end{aligned} \tag{43}$$

Proof. By employing the optimality condition, we obtain the following:

$$\begin{aligned}
\frac{\partial H}{\partial u_1} &= C_4 u_1 + \xi_1\beta\mathrm{SI} - \xi_2\beta\mathrm{SI},\\
\frac{\partial H}{\partial u_2} &= C_5 u_2 - \xi_2\rho E + \xi_4\rho E.
\end{aligned} \tag{44}$$

For the optimal control variables u_1^* and u_2^* that solve (44), we yield the following:

$$\begin{aligned}
u_1^*(t) &= \left\{\frac{(\xi_2 - \xi_1)\beta\mathrm{SI}}{C_4}\right\},\\
u_2^*(t) &= \left\{\frac{(\xi_2 - \xi_4)\rho E}{C_5}\right\}.
\end{aligned} \tag{45}$$

The optimality system can be written as follows:

$$\begin{aligned}
\frac{\mathrm{d}S^*}{\mathrm{d}t} &= \Lambda - \left(1 - \max\left\{\min\left\{\frac{(\xi_2 - \xi_1)\beta SI}{C_4}, 1\right\}, 0\right\}\right)\beta S^* I^* - \mu S^*,\\
\frac{\mathrm{d}E^*}{\mathrm{d}t} &= \left(1 - \max\left\{\min\left\{\frac{(\xi_2 - \xi_1)\beta SI}{C_4}, 1\right\}, 0\right\}\right)\beta S^* I^* - \left(\pi + \mu + \rho\max\left\{\min\left\{\frac{(\xi_2 - \xi_4)\rho E}{C_5}, 1\right\}, 0\right\}\right)E^*,\\
\frac{\mathrm{d}I^*}{\mathrm{d}t} &= \pi E^* - (\mu + \gamma + \psi + \eta)I^*,\\
\frac{\mathrm{d}Q^*}{\mathrm{d}t} &= \gamma(1 - \delta)I^* - (\tau + \phi + \mu)Q^* + \rho\max\left\{\min\left\{\frac{(\xi_2 - \xi_4)\rho E}{C_5}, 1\right\}, 0\right\}E^*,\\
\frac{\mathrm{d}H^*}{\mathrm{d}t} &= \psi I^* + \tau Q^* - (\kappa + \sigma + \mu)H^*,\\
\frac{\mathrm{d}R^*}{\mathrm{d}t} &= \phi Q^* + \delta\gamma I^* + \kappa H^* - \mu R^*.
\end{aligned} \tag{46}$$

□

8. Model with ABC-Fractional Derivative

This section expands upon the previously proposed model (1) by introducing fractional-order considerations using the ABC-fractional derivative. We utilize fixed-point theorems to assess both the existence and uniqueness of solutions within the generalized model. Prior to extending the model (1), a review of essential preliminary definitions will be conducted, proving beneficial for this section's analyses.

8.1. Preliminaries

Definition 9. The definition of ABC derivative and integration of function $z(t)$ are defined as

$$
\begin{aligned}
{}^{\mathrm{ABC}}D_{0+}^{\alpha} z(t) &= \frac{1-\alpha}{N(\alpha)} \int_0^t E_{\alpha}\left\{\frac{-\alpha}{1-\alpha}(t-x)^{\alpha}\right\} z'(x)\mathrm{d}x \\
{}^{\mathrm{ABC}}I_{0+}^{\alpha} z(t) &= \frac{1-\alpha}{N(\alpha)} z(t) + \frac{\alpha}{N(\alpha)\Gamma(\alpha)} \int_0^t (t-x)^{\alpha-1} z(x)\mathrm{d}x, \quad t > 0,
\end{aligned}
\tag{47}
$$

where α denotes fractional order. As a result, the suggested nonlinear fractional model in terms of the ABC-fractional operator has the following form:

$$
\begin{cases}
{}^{\mathrm{ABC}}D_0^{\alpha} S(t) = \Lambda - \beta \mathrm{SE} - \mu S, \\
{}^{\mathrm{ABC}}D_0^{\alpha} E(t) = \beta \mathrm{SE} - (\pi + \mu)E, \\
{}^{\mathrm{ABC}}D_0^{\alpha} I(t) = \pi E - (\mu + \gamma + \psi + \eta)I, \\
{}^{\mathrm{ABC}}D_0^{\alpha} Q(t) = \gamma(1-\delta)I - (\tau + \phi + \mu)Q, \\
{}^{\mathrm{ABC}}D_0^{\alpha} H(t) = \psi I(t) + \tau Q - (\kappa + \sigma + \mu)H, \\
{}^{\mathrm{ABC}}D_0^{\alpha} R(t) = \phi Q + \delta\gamma I + \kappa H - \mu R,
\end{cases}
\tag{48}
$$

with

$$
\begin{aligned}
S^0 &= S(0), \\
E^0 &= E(0), \\
I^0 &= I(0), \\
Q^0 &= Q(0), \\
H^0 &= H(0), \\
R^0 &= R(0).
\end{aligned}
\tag{49}
$$

8.2. Results for Existence and Uniqueness of the Model. In this section, the methodology of fixed-point theory is used to determine whether or not the suggested model has any solutions at all, as well as whether or not those solutions are unique. The Banach space denoted by the equation $E = C([0,T], R)$ is the space of all continuous real-valued functions with the norm provided by

$$
\|S, E, I, Q, H, R\| = \|S\| + \|E\| + \|I\| + \|Q\| + \|H\| + \|R\|.
\tag{50}
$$

Using the fractional operator ${}^{\mathrm{ABC}}I_{0+}^{\alpha}$ on both sides of the system (48), we get

$$
\begin{aligned}
S &= S_0 + \frac{1-\alpha}{N(\alpha)} G_1(t,S) + \frac{\alpha}{N(\alpha)\Gamma(\alpha)} \int_0^t (t-x)^{\alpha-1} G_1(x,S)\mathrm{d}x, \\
E &= E_0 + \frac{1-\alpha}{N(\alpha)} G_2(t,E) + \frac{\alpha}{N(\alpha)\Gamma(\alpha)} \int_0^t (t-x)^{\alpha-1} G_2(x,E)\mathrm{d}x, \\
I &= I_0 + \frac{1-\alpha}{N(\alpha)} G_3(t,I) + \frac{\alpha}{N(\alpha)\Gamma(\alpha)} \int_0^t (t-x)^{\alpha-1} G_3(x,I)\mathrm{d}x, \\
Q &= H_0 + \frac{1-\alpha}{N(\alpha)} G_4(t,Q) + \frac{\alpha}{N(\alpha)\Gamma(\alpha)} \int_0^t (t-x)^{\alpha-1} G_4(x,Q)\mathrm{d}x, \\
H &= H_0 + \frac{1-\alpha}{N(\alpha)} G_5(t,H) + \frac{\alpha}{N(\alpha)\Gamma(\alpha)} \int_0^t (t-x)^{\alpha-1} G_5(x,H)\mathrm{d}x, \\
R &= R_0 + \frac{1-\alpha}{N(\alpha)} G_6(t,R) + \frac{\alpha}{N(\alpha)\Gamma(\alpha)} \int_0^t (t-x)^{\alpha-1} G_6(x,R)\mathrm{d}x,
\end{aligned}
\tag{51}
$$

where

$$\begin{aligned} G_1(t,S) &= \Lambda - \beta SE - \mu S, \\ G_2(t,E) &= \beta SE - (\pi + \mu)E, \\ G_3(t,I) &= \pi E - (\mu + \gamma + \psi + \eta)I, \\ G_4(t,Q) &= \gamma(1-\delta)I - (\tau + \phi + \mu)Q, \\ G_5(t,H) &= \psi I + \tau Q - (\kappa + \sigma + \mu)H, \\ G_6(t,R) &= \phi Q + \delta\gamma I + \kappa H - \mu R. \end{aligned} \tag{52}$$

The kernels within (51) adhere to the Lipschitz condition for $0 \le \eta_i < 1, i = 1, 2, \ldots, 6$ if and only if the nonlinear functions S, E, I, Q, H, and R possess an upper bound. For instance, if S and S^* represent two functions, the outcome is as follows:

$$\begin{aligned} &\|G_1(t,S) - F_1(t,S^*)\| \\ &= \|\Lambda - \beta SE - \mu S - (\Lambda - \beta S^*(t)E - \mu S^*)\| \\ &= \|\mu(S^* - S) + \beta I(S^* - S)\| \\ &\le \left(\mu + \beta \sup_t \varepsilon[0,T]|E|\right)\|S - S^*\| \\ &= \eta_1 \|S - S^*\|, \end{aligned} \tag{53}$$

where $\eta_1 = (\mu + \beta \sup_t \varepsilon[0,T]|E|)$. Thus,

$$\|G_1(t,S) - G_1(t,S^*)\| \le \eta_1 \|S - S^*\|. \tag{54}$$

Similarly, repeat the same procedure as in (53) above, we yield

$$\begin{aligned} \|G_2(t,E) - G_2(t,E^*)\| &\le \eta_2 \|E - E^*\|, \\ \|G_3(t,I) - G_3(t,I^*)\| &\le \eta_3 \|I - I^*\|, \\ \|G_4(t,Q) - G_4(t,Q^*)\| &\le \eta_4 \|Q - Q^*\|, \\ \|G_5(t,H) - G_5(t,H^*)\| &\le \eta_5 \|H - H^*\|, \\ \|G_6(t,R) - G_6(t,R^*)\| &\le \eta_6 \|R - R^*\|. \end{aligned} \tag{55}$$

Here, η_i (where $i = 1, 2, \ldots, 6$) signifies the respective Lipschitz constant associated with the functions $G_i(\cdot)$ for $i = 1, 2, \ldots, 6$. Equation (51) can now be rephrased into a recursive form as demonstrated as follows:

$$\begin{aligned} S_n &= S_0 + \frac{1-\alpha}{N(\alpha)}G_1(t,S_{n-1}) + \frac{\alpha}{N(\alpha)\Gamma(\alpha)}\int_0^t (t-x)^{\alpha-1}G_1(x,S_{n-1})\mathrm{d}x, \\ E_n &= E_0 + \frac{1-\alpha}{N(\alpha)}G_2(t,E_{n-1}) + \frac{\alpha}{N(\alpha)\Gamma(\alpha)}\int_0^t (t-x)^{\alpha-1}G_2(x,E_{n-1})\mathrm{d}x, \\ I_n &= I_0 + \frac{1-\alpha}{N(\alpha)}G_3(t,I_{n-1}) + \frac{\alpha}{N(\alpha)\Gamma(\alpha)}\int_0^t (t-x)^{\alpha-1}G_3(x,I_{n-1})\mathrm{d}x, \\ Q_n &= Q_0 + \frac{1-\alpha}{N(\alpha)}G_4(t,Q_{n-1}) + \frac{\alpha}{N(\alpha)\Gamma(\alpha)}\int_0^t (t-x)^{\alpha-1}G_4(x,Q_{n-1})\mathrm{d}x, \\ H_n &= H_0 + \frac{1-\alpha}{N(\alpha)}G_5(t,H_{n-1}) + \frac{\alpha}{N(\alpha)\Gamma(\alpha)}\int_0^t (t-x)^{\alpha-1}G_5(x,H_{n-1})\mathrm{d}x, \\ R_n &= R_0 + \frac{1-\alpha}{N(\alpha)}G_6(t,R_{n-1}) + \frac{\alpha}{N(\alpha)\Gamma(\alpha)}\int_0^t (t-x)^{\alpha-1}G_6(x,R_{n-1})\mathrm{d}x. \end{aligned} \tag{56}$$

Let us represent the disparity between consecutive components as Φ_n^i, where $i = 1, 2, \ldots, 6$. Thus,

$$\Phi_n^1(t) = S_n - S_{n-1} = \frac{1-\alpha}{N(\alpha)}\left(G_1\left(t, S_{n-1} - G_2\left(t, S_{n-2}\right)\right)\right) + \frac{\alpha}{N(\alpha)\Gamma(\alpha)}\int_0^t (t-x)^{\alpha-1}\left(G_1\left(x, S_{n-1}(x)\right) - G_1\left(x, S_{n-2}\right)\right)\mathrm{d}x$$

$$\Phi_n^2(t) = E_n - E_{n-1} = \frac{1-\alpha}{N(\alpha)}\left(G_2\left(t, E_{n-1} - G_2\left(t, E_{n-2}\right)\right)\right) + \frac{\alpha}{N(\alpha)\Gamma(\alpha)}\int_0^t (t-x)^{\alpha-1}\left(G_2 x, E_{n-1}(x) - G_2\left(x, E_{n-2}\right)\right)\mathrm{d}x$$

$$\Phi_n^3(t) = I_n - I_{n-1} = \frac{1-\alpha}{N(\alpha)}\left(G_3\left(t, I_{n-1} - G_3\left(t, I_{n-2}\right)\right)\right) + \frac{\alpha}{N(\alpha)\Gamma(\alpha)}\int_0^t (t-x)^{\alpha-1}\left(G_3\left(x, I_{n-1}(x)\right) - G_3\left(x, I_{n-2}\right)\right)\mathrm{d}x$$

$$\Phi_n^4(t) = Q_n - Q_{n-1} = \frac{1-\alpha}{N(\alpha)}\left(G_4\left(t, Q_{n-1} - G_4\left(t, Q_{n-2}\right)\right)\right) + \frac{\alpha}{N(\alpha)\Gamma(\alpha)}\int_0^t (t-x)^{\alpha-1}\left(G_4\left(x, Q_{n-1}(x)\right) - G_4\left(x, Q_{n-2}\right)\right)\mathrm{d}x$$

$$\Phi_n^5(t) = H_n - H_{n-1} = \frac{1-\alpha}{N(\alpha)}\left(G_5\left(t, H_{n-1} - G_5\left(t, H_{n-2}\right)\right)\right) + \frac{\alpha}{N(\alpha)\Gamma(\alpha)}\int_0^t (t-x)^{\alpha-1}\left(G_5\left(x, H_{n-1}(x)\right) - G_5\left(x, H_{n-2}\right)\right)\mathrm{d}x$$

$$\Phi_n^6(t) = R_n - R_{n-1} = \frac{1-\alpha}{N(\alpha)}\left(G_6\left(t, R_{n-1} - G_6\left(t, R_{n-2}\right)\right)\right) + \frac{\alpha}{N(\alpha)\Gamma(\alpha)}\int_0^t (t-x)^{\alpha-1}\left(G_6\left(x, R_{n-1}(x)\right) - G_6\left(x, R_{n-2}\right)\right)\mathrm{d}x. \tag{57}$$

Taking into consideration that $S_n = \sum_{i=0}^1 \Phi_i^1, E_n = \sum_{i=0}^1 \Phi_i^1, I_n = \sum_{i=0}^1 \Phi_i^1, Q_n = \sum_{i=0}^1 \Phi_i^1, H_n = \sum_{i=0}^1 \Phi_i^1, \quad R_n = \sum_{i=0}^1 \Phi_i^1$. Taking the norm on both sides of (56) and using the (57) yield

$$\begin{aligned}
\|\Phi_n^1\| &= \frac{1-\alpha}{N(\alpha)}\eta_1\|\Phi_{n-1}^1\| \frac{\alpha\eta_1}{N(\alpha)\Gamma(\alpha)}\int_0^t (t-x)^{\alpha-1}\|\Phi_{n-1}^1\|\mathrm{d}x,\\
\|\Phi_n^2\| &= \frac{1-\alpha}{N(\alpha)}\eta_2\|\Phi_{n-1}^2\| \frac{\alpha\eta_2}{N(\Re)\Gamma(\alpha)}\int_0^t (t-x)^{\alpha-1}\|\Phi_{n-1}^2\|\mathrm{d}x,\\
\|\Phi_n^3\| &= \frac{1-\alpha}{N(\alpha)}\eta_3\|\Phi_{n-1}^3\| \frac{\alpha\eta_3}{N(\Re)\Gamma(\alpha)}\int_0^t (t-x)^{\alpha-1}\|\Phi_{n-1}^3\|\mathrm{d}x,\\
\|\Phi_n^4\| &= \frac{1-\alpha}{N(\alpha)}\eta_4\|\Phi_{n-1}^4\| \frac{\alpha\eta_4}{N(\Re)\Gamma(\alpha)}\int_0^t (t-x)^{\alpha-1}\|\Phi_{n-1}^4\|\mathrm{d}x,\\
\|\Phi_n^5\| &= \frac{1-\alpha}{N(\alpha)}\eta_5\|\Phi_{n-1}^5\| \frac{\alpha\eta_5}{N(\Re)\Gamma(\alpha)}\int_0^t (t-x)^{\alpha-1}\|\Phi_{n-1}^5\|\mathrm{d}x,\\
\|\Phi_n^6\| &= \frac{1-\alpha}{N(\alpha)}\eta_6\|\Phi_{n-1}^6\| \frac{\alpha\eta_6}{N(\Re)\Gamma(\alpha)}\int_0^t (t-x)^{\alpha-1}\|\Phi_{n-1}^6\|\mathrm{d}x.
\end{aligned} \tag{58}$$

Based on the preceding conclusions, we are now able to formulate and prove the main theorem.

Theorem 10. *The fractional proposed model (32) possesses a unique solution for* $t\varepsilon[0,T]$ *if the condition is satisfied*

$$\left(\frac{1-\alpha}{N(\alpha)}\eta_i + \frac{\eta_i}{N(\alpha)\Gamma(\alpha)}T^{\alpha}\right) < 1, \quad i = 1, 2, 3, \ldots, 6. \tag{59}$$

Proof. Because the functions S, E, I, Q, H, R are limited by the assumptions, they satisfy the Lipschitz condition. In light of equation (40), we get

$$\begin{aligned}
\|\Phi_n^1\| &\le \|S_n(0)\|\left(\frac{1-\alpha}{N(\alpha)}\eta_1 + \frac{\eta_1}{N(\alpha)\Gamma(\alpha)}T^{\alpha}\right)^n,\\
\|\Phi_n^2\| &\le \|E_n(0)\|\left(\frac{1-\alpha}{N(\alpha)}\eta_2 + \frac{\eta_2}{N(\alpha)\Gamma(\alpha)}T^{\alpha}\right)^n,\\
\|\Phi_n^3\| &\le \|I_n(0)\|\left(\frac{1-\alpha}{N(\alpha)}\eta_3 + \frac{\eta_3}{N(\alpha)\Gamma(\alpha)}T^{\alpha}\right)^n,\\
\|\Phi_n^4\| &\le \|Q_n(0)\|\left(\frac{1-\alpha}{N(\alpha)}\eta_4 + \frac{\eta_4}{N(\alpha)\Gamma(\alpha)}T^{\alpha}\right)^n,\\
\|\Phi_n^5\| &\le \|H_n(0)\|\left(\frac{1-\alpha}{N(\alpha)}\eta_5 + \frac{\eta_5}{N(\alpha)\Gamma(\alpha)}T^{\alpha}\right)^n,\\
\|\Phi_n^6\| &\le \|R_n(0)\|\left(\frac{1-\alpha}{N(\alpha)}\eta_6 + \frac{\eta_6}{N(\alpha)\Gamma(\alpha)}T^{\alpha}\right)^n.
\end{aligned} \tag{60}$$

As a result, the above sequences occur and as $n \longrightarrow \infty, \|\Phi_n^i(t)\| \longrightarrow 0, i = 1, 2, \ldots 6$. In addition, using the triangle inequality for each k, we obtain

$$\begin{aligned}
\|S_{n+k} - S_n\| &\le \sum_{i=n+1}^{n+k} Z_1^i = \frac{Z_1^{n+1} - Z_1^{n+k+1}}{1 - Z_1},\\
\|E_{n+k} - E_n\| &\le \sum_{i=n+1}^{n+k} Z_2^i = \frac{Z_2^{n+1} - Z_2^{n+k+1}}{1 - Z_2},\\
\|I_{n+k} - I_n\| &\le \sum_{i=n+1}^{n+k} Z_3^i = \frac{Z_3^{n+1} - Z_3^{n+k+1}}{1 - Z_3},\\
\|Q_{n+k} - Q_n\| &\le \sum_{i=n+1}^{n+k} Z_4^i = \frac{Z_4^{n+1} - Z_4^{n+k+1}}{1 - Z_4},\\
\|H_{n+k} - H_n\| &\le \sum_{i=n+1}^{n+k} Z_5^i = \frac{Z_5^{n+1} - Z_5^{n+k+1}}{1 - Z_5},\\
\|R_{n+k} - R_n\| &\le \sum_{i=n+1}^{n+k} Z_6^i = \frac{Z_6^{n+1} - Z_5^{n+k+1}}{1 - Z_6}.
\end{aligned} \tag{61}$$

In (60), the expressions within the brackets are denoted as Z_i, where $i = 1, 2, \ldots, 6$. The condition $(1 - \alpha/N(\alpha)\eta_i + \eta_i/N(\alpha)\Gamma(\alpha)T^{\alpha}) < 1$ is imposed. As per the uniform convergence theorem, the functions S_n, E_n, I_n, Q_n, H_n, and R_n constitute a Cauchy sequence in E. Employing the limit theory on (56) as $n \longrightarrow \infty$, we observe that the limit of these sequences corresponds to the unique solution of the proposed model (48). □

Table 2: Parameters and their values.

Name	Parameter values	References
β	0.0805	[23]
μ	0.0106	[23]
π	0.0668	[23]
γ	0.0002	[23]
δ	0.07	Fiffted
Λ	0.5	Fiffted
ϕ	0.03668	Assumed
η	0.28	Fiffted
σ	0.02537	[23]
ψ	0.0045	Assumed
τ	0.000428	Demographic

9. Numerical Simulation

We employ numerical simulations to demonstrate the theoretical findings reported in earlier sections. Days are used as the time unit. The parameters determined and fitted in Table 2 are examined, and Figures 5–8 are generated. The influence of control variables on the model (1) is graphically shown in Figure 7.

Figures 5(a)–5(f) depict the behavior of susceptible persons S, exposed people E, infected people I, quarantined people Q, hospitalised people H, and recovered people R for different fractional-order α values. Figure 5(a) indicates that when the value of α falls, the number of sensitive people falls quickly and converges to zero. The graph in Figure 5(b) for exposed individuals shows that when the value of α declines, so does the rate of increase. Figure 5(c) shows that the infected population rises fast with noninteger values of α, but when the value of α decreases, the rate of infection increases. It also indicates that the number of infected persons is much smaller at a very slow rate ($\alpha = 0.8$). The number of patients quarantined $Q(t)$ and hospitalised $H(t)$ reduces as α increases, as seen in Figures 5(d) and 5(e), respectively. Similarly, persons are retrieved or eliminated (dead) extremely quickly with a change in α, as seen in Figure 5(f).

We provide numerical simulations of the suggested model (1) and (31) with and without optimum control. For this objective, a MATLAB programme was designed to combine the essential optimality requirements, and a detailed output is extensively tested using a variety of simulations. As discussed in Section 7, the optimality system for the proposed optimal control problem is derived from the state and adjoint equations under proper boundary conditions. We showed classical derivative solutions in Figures 6(a)–6(f) by a red line to compare with approximation solutions using optimum controls and found that both solutions are almost equivalent for each population $Q(t)$. We depict the susceptible people of systems (1) and (31) in Figure 6(a). The red line represents the population of class S in the uncontrolled system (1), whereas the green solid line represents the population of class S in the regulated system (31), with optimum regulations. The exposed population of both systems (1) and (31) is shown in Figure 6(b). When no control measures are taken, the red solid line indicates that there are more exposed persons. Figure 6(c) depicts the infectious population I of system (1) without

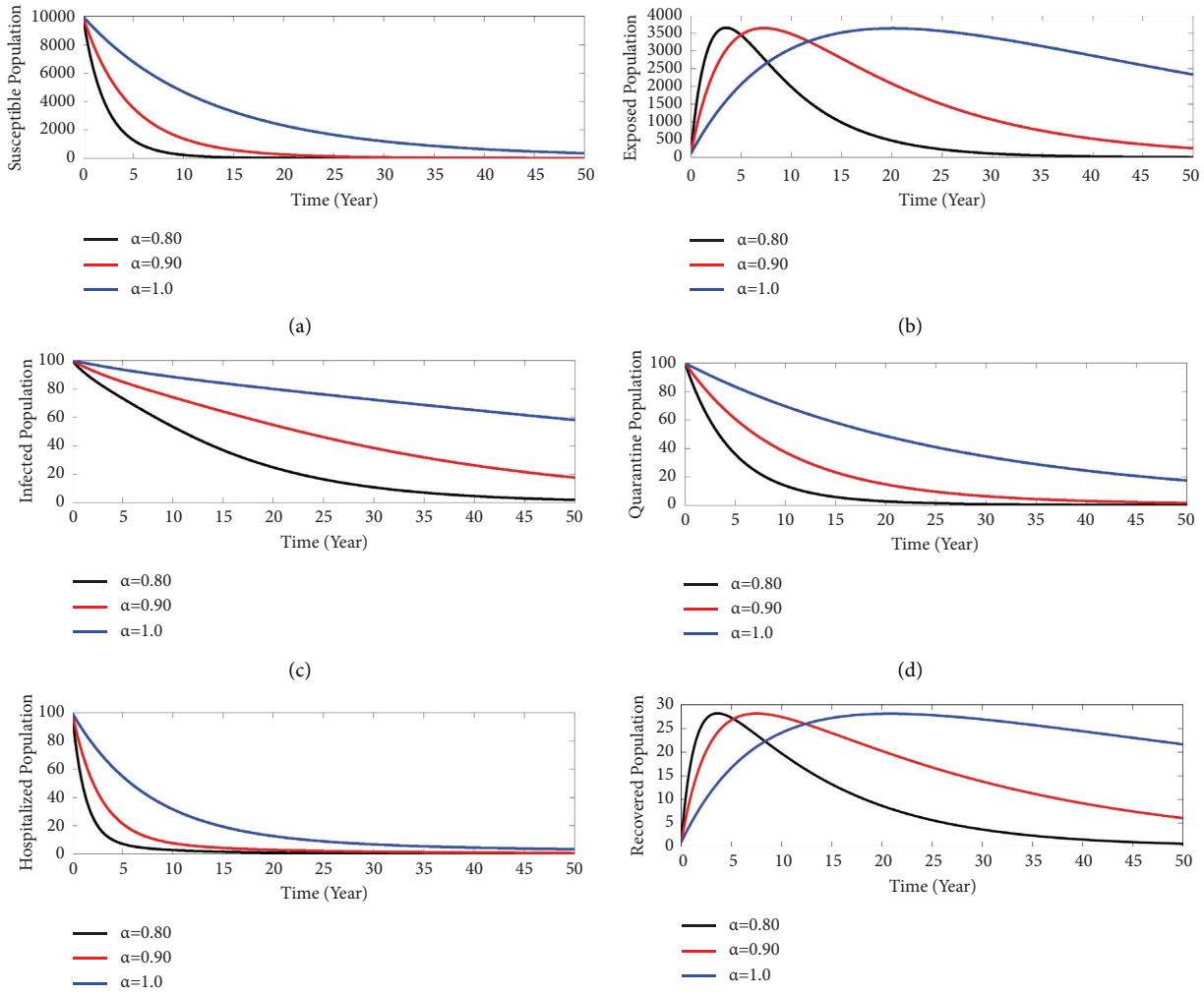

Figure 5: The dynamical behavior of the fractional model (1) with $\alpha = 0.8$, 0.9, and 1.

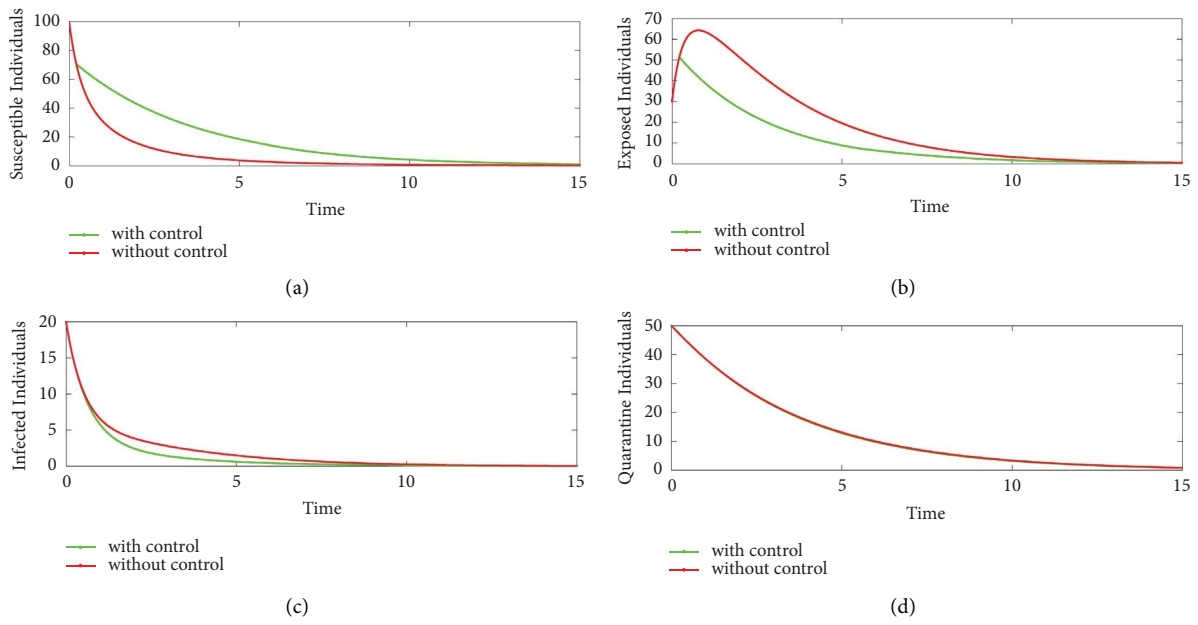

Figure 6: Continued.

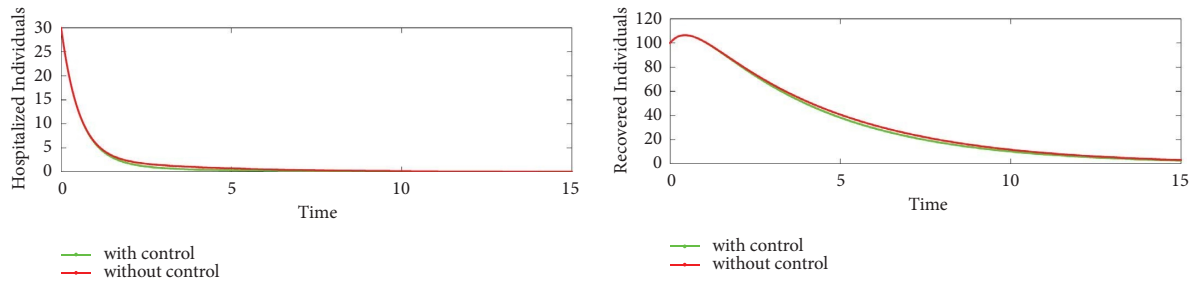

(e) (f)

Figure 6: Graphical representation of the model (1) with and without controls.

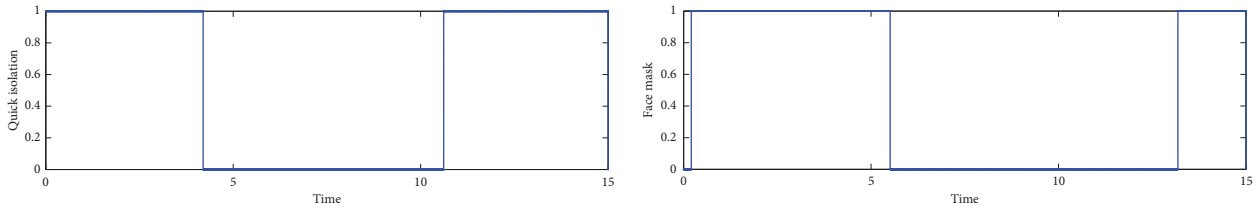

(a) (b)

Figure 7: Numerical simulations of the control variables.

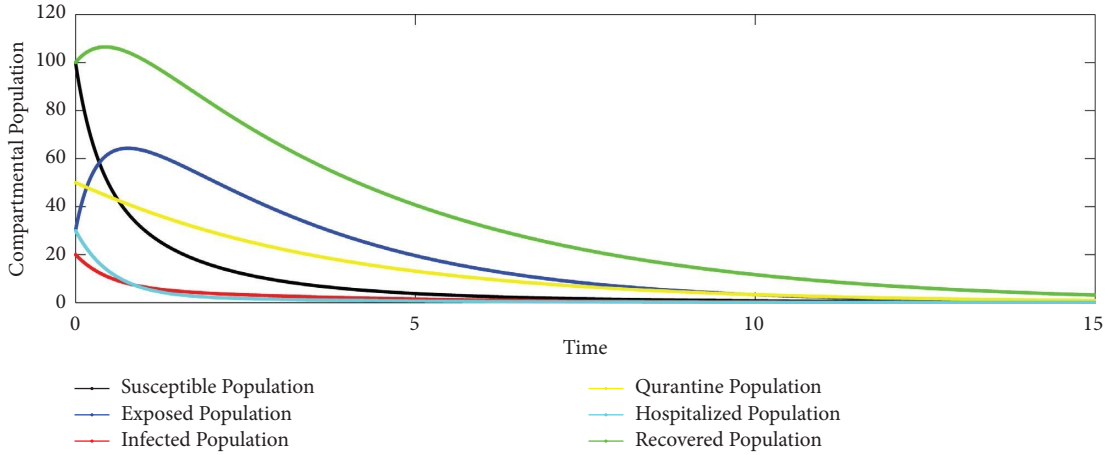

Figure 8: Graphical representation of all the classes of our developed model under integer-order derivative.

controls and system (31) with controls. The red solid line indicates that when no control is adopted, there are more infectious persons.

The hospitalised population $H(t)$ with and without controls is shown in Figure 6(e). When all controls are implemented, the green solid line indicates that fewer people are hospitalised. Finally, Figure 6(f) depicts the reconstructed population $R(t)$. There are more recovered people in the example that employs optimum control theory (because there is more susceptible, exposed, hospitalised, quarantined, and infected).

10. Conclusion

In this study, we formulated a mathematical model to explore the transmission dynamics of the novel coronavirus infection (COVID-19) and the factors influencing its spread among individuals. Leveraging the principles of mathematical epidemiology, we modeled the progression of susceptibility to infection and subsequent recovery pathways. Upon confirming the model's positivity and boundedness, we computed the basic reproduction number using the next-generation matrix method. We established the local and global stability of disease equilibria. Employing an integer-order model, we applied optimal control strategies to address the COVID-19 epidemic.

Utilizing two control measures—social distancing and mask usage, along with prompt actions to protect the vulnerable population and quarantine for exposed individuals—we aimed to curtail viral transmission globally. We discussed the necessary conditions for an optimal control problem and aimed to diminish the number of vulnerable and infected individuals while enhancing the count of

recoveries in the COVID-19 scenario. Employing Pontryagin's maximum principle, we determined the optimal values for the proposed controls. The resulting optimality system was numerically solved using the MATLAB computing environment.

Our model visually depicts the transmission dynamics of the virus through contact and assesses the pace of change by tracking the number of infections and the likelihood of future infections. The epidemic is fueled by new infections, prompting our research to contribute to future pandemic predictions. We explored the stability related to the reproductive number, illustrating the impact of interactions between infected and susceptible populations. Regulating this contact rate proves pivotal in controlling the current disease spread. Diverse regulations govern public gatherings across states and regions, necessitating adherence to guidelines to mitigate health risks effectively.

Data Availability

The data supporting the current study are available from the corresponding author upon request.

Conflicts of Interest

The authors declare that there are no conflicts of interest.

Authors' Contributions

All authors contributed equally to this work.

Acknowledgments

All authors have agreed to submit this version.

References

[1] W. H. Organization et al., *Novel Coronavirus (2019-ncov), situation report*, vol. 3.

[2] D. Kumar, R. Malviya, and P. K. Sharma, "Corona virus: a review of COVID-19," *EJMO*, vol. 4, no. 1, pp. 8–25, 2020.

[3] A. Çalıca Utku, G. Budak, O. Karabay, E. Güçlü, H. D. Okan, and A. Vatan, "Main symptoms in patients presenting in the COVID-19 period," *Scottish Medical Journal*, vol. 65, no. 4, pp. 127–132, 2020.

[4] B. Fatima, M. Yavuz, M. U. Rahman, and F. S. Al-Duais, "Modeling the epidemic trend of middle eastern respiratory syndrome coronavirus with optimal control," *Mathematical Biosciences and Engineering*, vol. 20, no. 7, pp. 11847–11874, 2023.

[5] C. Fernández-de Las-Peñas, D. Palacios-Ceña, V. Gómez-Mayordomo et al., "Prevalence of post-COVID-19 symptoms in hospitalized and non-hospitalized COVID-19 survivors: a systematic review and meta-analysis," *European Journal of Internal Medicine*, vol. 92, pp. 55–70, 2021.

[6] C. Castillo-Chavez and B. Song, "Dynamical models of tuberculosis and their applications," *Mathematical Biosciences and Engineering*, vol. 1, no. 2, pp. 361–404, 2004.

[7] M. Roser, H. Ritchie, E. Ortiz-Ospina, and J. Hasell, "Coronavirus pandemic (COVID-19), Our world in data," https://ourworldindata.org/coronavirus.

[8] B. Fatima, M. Yavuz, M. ur Rahman, A. Althobaiti, and S. Althobaiti, "Predictive modeling and control strategies for the transmission of middle east respiratory syndrome coronavirus," *Mathematical and Computational Applications*, vol. 28, no. 5, p. 98, 2023.

[9] M. U. Rahman, Y. Karaca, R. P. Agarwal, and S. Adriani David, "Mathematical modelling with computational fractional order for the unfolding dynamics of the communicable diseases," *Applied Mathematics in Science and Engineering*, vol. 32, no. 1, 2024.

[10] B. Li, Z. Eskandari, and Z. Avazzadeh, "Dynamical behaviors of an sir epidemic model with discrete time," *Fractal and Fractional*, vol. 6, no. 11, p. 659, 2022.

[11] M. Ur Rahman, G. Alhawael, and Y. Karaca, "Multi-compartmental analysis of middle eastern respiratory syndrome coronavirus model under fractional operator with next-generation matrix methods," *Fractals*, vol. 31, no. 10, pp. 2340093–2412360, 2023.

[12] I. U. Haq, N. Ali, H. Ahmad, and T. A. Nofal, "On the fractional-order mathematical model of COVID-19 with the effects of multiple non-pharmaceutical interventions," *AIMS Mathematics*, vol. 7, no. 9, pp. 16017–16036, 2022.

[13] I. U. Haq, N. Ali, and K. S. Nisar, "An optimal control strategy and Grünwald-letnikov finite-difference numerical scheme for the fractional-order COVID-19 model," *Mathematical Modelling and Numerical Simulation with Applications*, vol. 2, no. 2, pp. 108–116, 2022.

[14] C. Yang and J. Wang, "A mathematical model for the novel coronavirus epidemic in Wuhan, China," *Mathematical Biosciences and Engineering*, vol. 17, no. 3, pp. 2708–2724, 2020.

[15] M.-T. Li, G.-Q. Sun, J. Zhang et al., "Analysis of COVID-19 transmission in Shanxi Province with discrete time imported cases," *Mathematical Biosciences and Engineering*, vol. 17, no. 4, pp. 3710–3720, 2020.

[16] C. N. Ngonghala, E. Iboi, S. Eikenberry et al., "Mathematical assessment of the impact of non-pharmaceutical interventions on curtailing the 2019 novel Coronavirus," *Mathematical Biosciences*, vol. 325, 2020.

[17] S. E. Eikenberry, M. Mancuso, E. Iboi et al., "To mask or not to mask: modeling the potential for face mask use by the general public to curtail the COVID-19 pandemic," *Infectious disease modelling*, vol. 5, pp. 293–308, 2020.

[18] I. U. Haq, M. Yavuz, N. Ali, and A. Akgül, "A SARS-Cov-2 fractional-order mathematical model via the modified euler method," *Mathematical and Computational Applications*, vol. 27, no. 5, p. 82, 2022.

[19] I. U. Haq, N. Ullah, N. Ali, and K. S. Nisar, "A new mathematical model of COVID-19 with quarantine and vaccination," *Mathematics*, vol. 11, no. 1, p. 142, 2022.

[20] P. Samui, J. Mondal, and S. Khajanchi, "A mathematical model for COVID-19 transmission dynamics with a case study of India," *Chaos, Solitons & Fractals*, vol. 140, 2020.

[21] F. Özköse, M. Yavuz, M. T. Şenel, and R. Habbireeh, "Fractional order modelling of omicron SARS-Cov-2 variant containing heart attack effect using real data from the United Kingdom," *Chaos, Solitons & Fractals*, vol. 157, 2022.

[22] I. U. Haq, N. Ali, S. Ahmad, and T. Akram, "A hybrid interpolation method for fractional PDEs and its applications to fractional diffusion and buckmaster equations," *Mathematical Problems in Engineering*, vol. 2022, Article ID 2517602, 12 pages, 2022.

[23] I. Ahmed, G. U. Modu, A. Yusuf, P. Kumam, and I. Yusuf, "A mathematical model of Coronavirus Disease (COVID-19) containing asymptomatic and symptomatic classes," *Results in Physics*, vol. 21, 2021.